Nitrogen and Argon Adsorption and SEM Characterization of C_{60} and C_{60}/C_{70} Fullerenes: Comparison with Graphite

Vladimir Yu. Gusev,*,† Sigrid Ruetsch,† Ludwig A. Popeko,‡ and Ilya E. Popeko§

TRI/Princeton, P.O. Box 625, Princeton, New Jersey 08542, Neutrino Physics Laboratory, St. Petersburg Institute of Nuclear Physics, Gatchina, St. Petersburg District, 188350, Russia, and Semi-Alloys Company, 888 South Columbus Avenue, Mount Vernon, New York 10550

Received: March 30, 1999; In Final Form: June 4, 1999

The surface and pore structure properties of the C_{60} and C_{60}/C_{70} fullerene powders were studied by means of scanning electron microscopy, helium pycnometry, and 77.4 K nitrogen and argon adsorption. The pore structure of fullerene powders is macroporous and consists mainly of the voids between the fullerene aggregates. In the major part of the adsorption monolayer, both nitrogen and argon interactions with fullerenes are weaker than with graphite, possibly because of the reduction of the gas molecule−mirror image effect in the case of fullerenes. In Henry's law limit, however, nitrogen and argon adsorption on fullerenes is quantitatively similar to that on graphite because of the adsorption potential enhancement in the spaces between the surface fullerene molecules. In the multilayer regime, nitrogen adsorption on both fullerenes becomes similar to that on graphite. Both fullerenes behave similarly with respect to the adsorption of the studied gases.

Introduction

The research and development interest in the buckminsterfullerenes (bf)[1] sharply increased once the means of their mass production was developed.[2] The adsorption properties of the bf make them suitable for deployment in the bf-based adsorbents,[3] surface acoustic wave devices,[4] gas sensors,[5] stationary phases for gas chromatography,[6] and gas membranes.[7] The understanding of the nature of solid−fluid interactions is gained by studying the model materials with a reliably known structure (see, e.g., ref 8). One of the most important goals of such studies is the determination of the fluid-solid potential energy function.[8,9] It is desirable for this purpose to use a model adsorbent with a surface, which is uniform at a molecular scale, simple (nonporous) geometry, and considerable and well-determined surface area.

In the case of carbonaceous materials, graphitized carbon black (gcb) was used to this end for decades.[8,10] The properties of gas−solid interactions on gcb are well known and used in practical applications, such as characterization and prediction of adsorption properties of heterogeneous activated carbons on the basis of molecular theory, simulations,[11,12] and empirical approaches.[10] The gcb surface is prepared by high-temperature treatment of the initially heterogeneous carbons, during which the irregular surface of the solid is restructured into the graphite basal planes.[13] The homogeneity of the gcb surface, however, depends on graphitization temperature[13] and may contain several types of adsorption sites in small amounts.[14−17]

The C_{60} and C_{70} are the most abundant bf forms and make up the main component of the fullerite soot. In contrast to graphite, the bf can be obtained as molecular crystals without heat treatment. When crystallized from solutions, both C_{60} and C_{60}/C_{70} binary phases form either ordered face-centered cubic or hexagonal close-packed structures, which persist across the wide concentration intervals (see, e.g., ref 18 and references therein). The molecular regularity of the bf surface is suggested by atom force microscopy.[19] Surprisingly, despite the large amount of research devoted to bf, only a few adsorption studies of this material were reported. They, however, reveal a variety of gas behaviors on the bf surface. The measurements of helium adsorption on C_{60}/C_{70} bf[20] showed that helium might intercalate into the bf crystal. Subjecting bf films to the oxygen atmosphere was shown to reversibly change their electric conductivity.[21] Supercritical carbon dioxide adsorption measurements showed that the CO_2 molecules might slowly intercalate into the bulk of the solid under high gas pressure and affect its crystal structure.[22] The IR spectra of carbon monoxide and nitrogen oxide adsorbed on C_{60} film revealed two regular types of adsorption sites,[23] those located in the voids between and on top of C_{60} molecules.[24] The authors of the measurements of 77 K nitrogen adsorption on bf crystals suggest that recrystallization-induced microporous structure may exist in the amount of less than one volume percent on the surface of the bf crystal.[25,26]

A fundamental distinction between interactions of fluids with the bf and gcb surfaces is that the former should better conform to a widely employed theoretical assumption of the pair additivity of the fluid−solid interactions (see e.g., ref 8). While locally the carbon atoms in bf and gcb have similar electronic structures (since the relevant electron orbitals are in the p_z states in both cases), the electron conductivity of undoped bf is 11 orders of magnitude lower than that of the graphite layer.[1] Therefore, the effect of the gas atom−surface mirror image interactions[27,28] that may account for up to one-third of the gas−solid interactions in gcb may be greatly reduced in bf. One of the goals of this investigation was to address this issue by macroscopic experimental measurements of the nitrogen and argon adsorption on the bf surface in sub-, mono- and multilayer regimes.

* To whom correspondence should be addressed. Present address: CuraGen Corporation, 555 Long Wharf Drive, New Haven, CT 06511. E-mail: vgusev@curagen.com.

† TRI/Princeton.

‡ St. Petersburg Institute of Nuclear Physics.

§ Semi-Alloys Company.

10.1021/jp991081s CCC: $18.00
Published on Web 07/14/1999

Experimental

Materials. The C_{60} fullerenes were supplied by Dynamic Enterprises, Ltd. (Twyford, U.K.) and had quoted purity of 99.5%.

The C_{60}/C_{70} bf were synthesized and initially characterized at Neutrino Physics Laboratory of St. Petersburg Institute of Nuclear Physics (PINP, Russia), and provided by courtesy of the U.S. distributor, Semi-Alloys Co. (NY). The synthesis was based on a standard technique of burning the graphite electrodes in helium atmosphere at 150−200 Torr in the original high output setup designed and built at PINP. To maintain the purity of the helium atmosphere, melting lithium absorber was permanently placed in the reactor. After burning one thousand graphite electrodes, accumulated soot was transferred into a 200-liter container, where it was vacuumed down to 0.1 Torr, producing 5 kg of soot containing 8.5% of fullerenes. Fullerene mixture was then extracted from the soot by washing it with *o*-xylene then filtrating and evaporating the solvent. Used *o*-xylene was recycled. Composition of the fullerenes was determined by high performance liquid chromatography. The C_{60}/C_{70} ratio was 76:22, heavier fullerenes and impurities comprised less than 2%, including carbon soot (less than 1%) and oil (less than 0.1%). The temperature of bf sublimation in a vacuum was determined to be 200 °C. The flash point in air was determined to be 600 °C by the standard burning front temperature technique.

Electron Microscopy. The scanning electron microscopy of bf powders was carried out in a Hitachi S-4500 digital field emission scanning electron microscope. A small amount of the bf powder was placed on a clean glass slide. Double-sided carbon tape was placed on the surface of an SEM stub and the stub was inverted in such a manner that the free side of the carbon tape gently picked-up a small amount of the carbon powder off the glass slide. The sample was then coated with an 80 Å layer of platinum to obtain better contrast and provide improved cohesion to the poorly cohering clusters of bf aggregates.

The substrate was extremely sensitive to the electron beam, and the fullerene clusters disintegrated at high accelerating voltage. Therefore, the scanning was carried out at a long working distance (27 mm) and low accelerating voltage (1 to 5 kV) to minimize the beam damage to the substrate. To optimize the contrast and obtain a stronger signal, the accelerating voltage was increased from 1 and 2 kV to 5 kV. Here, 5 kV at long working distance was the highest voltage affordable without exposing the sample to excessive beam damage. However, even under these conditions, the samples tended to collapse into darkness and displayed spontaneous dislodging of complete particle aggregates from the weakly cohering bf clusters. Severe drifting or moving of the bf particles was a common phenomenon, observed at low as well as high magnification, and is consistent with the weak nature of the van der Waals bond acting between the fullerene molecules. To minimize the charge-up effect, the images were recorded by integrating frames taken at a very short exposure time.

Adsorption Measurements. The adsorption experiments were done in two laboratories using the automatic volumetric apparati Autosorb 1C (Quantachrome Corp.) and ASAP 2010 (Micromeritics Inc.), for nitrogen and argon measurements, respectively. The bf samples were outgassed at 150 °C for 24 h at pressure below 10^{-3} Torr prior to the gas adsorption measurements. All measurements were done at pressures of 10^{-3} to 760 Torr and temperature 77.4 K; the latter was maintained using a liquid nitrogen bath.

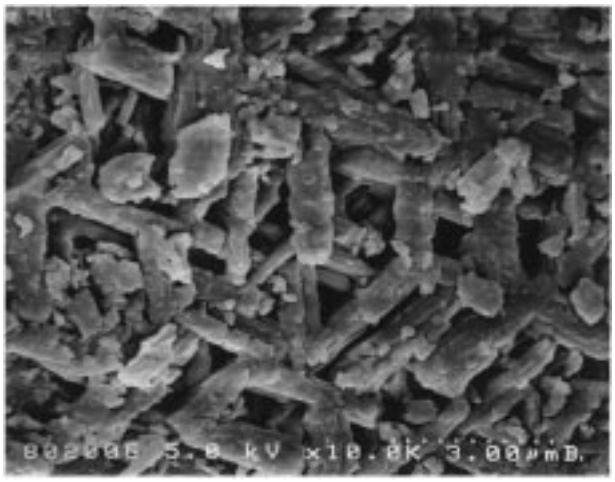

Figure 1. SEM image of C_{60} bf powder.

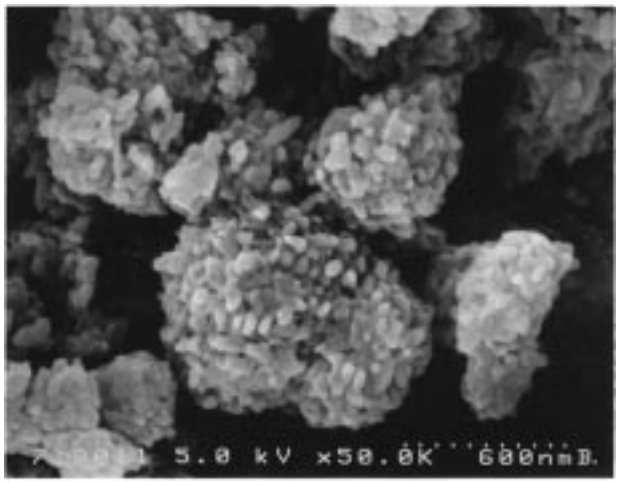

Figure 2. SEM image of C_{60}/C_{70} bf powder.

Helium Pycnometry. The bf densities $\rho_{C60/C70} = 1.64$ g/cm^3 and $\rho_{C60} = 1.65$ g/cm^3 were determined in the adsorption instrument at room temperature by helium displacement over the outgassed bf samples.

Gases. Nitrogen, argon, and helium (National Compressed Gases, Inc.) had quoted purity of better than 99.97% and were used without further purification.

Results and Discussion

The SEM images and nitrogen and argon adsorption isotherms yield structural characteristics of bf at the overlapping geometrical scales. The bf SEM images (Figures 1 and 2) allow analyzing the structure of the powders down to the 30-nm range. The C_{60} bf powder (Figure 1) consisted mostly of elongated particles in μm size range. The C_{60}/C_{70} primary particles (Figure 2) are of spherical or elliptical shape ranging in size from 30 to 80 nm. These grains form secondary well-cohering (even under the SEM conditions) round aggregates, which may range in size from 200 to 800 nm. The secondary bf aggregates, in turn, form weakly cohering several μm-wide clusters.

The density of the bf powders determined by helium pycnometry is characteristic of its composition.[29] Since helium may intercalate into the bf crystals,[20] the bf density $\rho_{C60/C70} = 1.64$ g/cm^3 and $\rho_{C60} = 1.65$ g/cm^3, determined in this work, may be considered as the upper bound for the density of the bf crystal. This is in agreement with the C_{60} bf crystal density reported as 1.65 g/cm^3,[29] and is considerably smaller than the graphite density (2.172 g/cm^3).

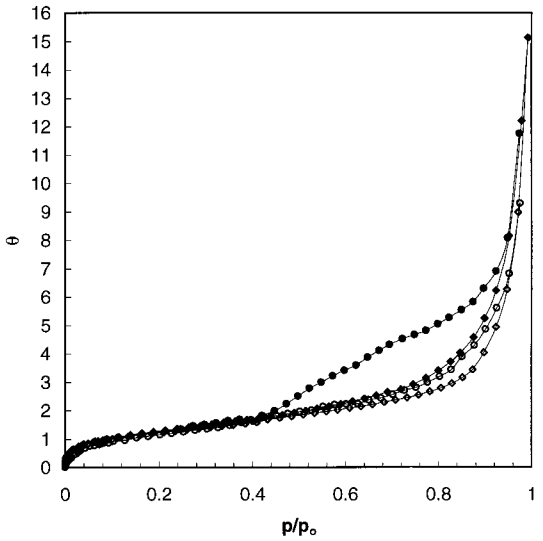

Figure 3. Nitrogen adsorption isotherms on bf at 77.4 K. Adsorption θ is expressed in units of n_m determined from the BET equation. Circles, C_{60}; diamonds, C_{60}/C_{70} bf. Open symbols, adsorption; closed symbols, desorption.

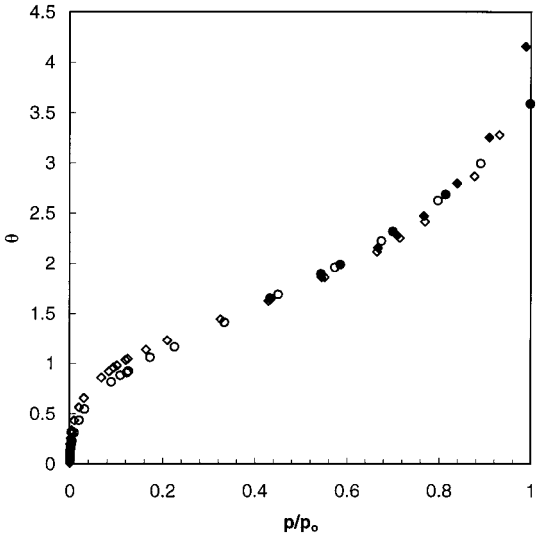

Figure 4. Argon adsorption isotherms on bf at 77.4 K. Legend is the same as in Figure 3.

The nitrogen and argon adsorption isotherms on both bf (Figures 3 and 4) belong to a type IV of the IUPAC classification and allow characterizing the bf surface and porous structure at scales of tenths to hundreds of nm.[10] The adsorption isotherms of this type are amenable to the BET analysis.[30] The experimental data represented in the form of the BET coordinates plot (Figures 5 and 6) could be linearized in the p/p_o relative pressure range of 0.05 to 0.32 for both samples and gases. The constant C of the BET equation, which is related to the characteristic adsorption energy in the first monolayer, was determined to be $C_{C60}(N_2) = 60$ and $C_{C60/C70}(N_2) = 85$ in the case of nitrogen and $C_{C60}(Ar) = 30$ and $C_{C60/C70}(Ar) = 70$ in the case of argon. This characterizes both bf samples as weaker than gcb ($C_{gcb}(N_2) = 150$,[31] $C_{gcb}(Ar) = 320$, estimated from experimental data[13]). The C_{60} and C_{60}/C_{70} monolayer capacities n_m determined from the above fits were 0.010 and 0.117 mmol/g in the case of nitrogen and 0.0116 and 0.124 mmol/g in the case of argon. The latter values were used to estimate the bf BET surface area $A^{BET}_{C60}(N_2) = 1.0$ m^2/g, $A^{BET}_{C60/C70}(N_2) = 11.7$ m^2/g and $A^{BET}_{C60}(Ar) = 0.96$ m^2/g, $A^{BET}_{C60/C70}(Ar) = 10.7$ m^2/g. Here, the cross-sectional molecular area a_m was assumed to be 0.162 nm^2 and 0.138 nm^2 in the nitrogen and argon monolayers, respectively. The latter values are often chosen for the adsorption of nitrogen on different substrates including gcb and adsorption of argon on gcb.[10] The value of the surface area of the C_{60}/C_{70} sample is remarkably close to the surface area values reported for some gcb (see e.g. ref 15), and makes this bf especially suitable for routine measurements.

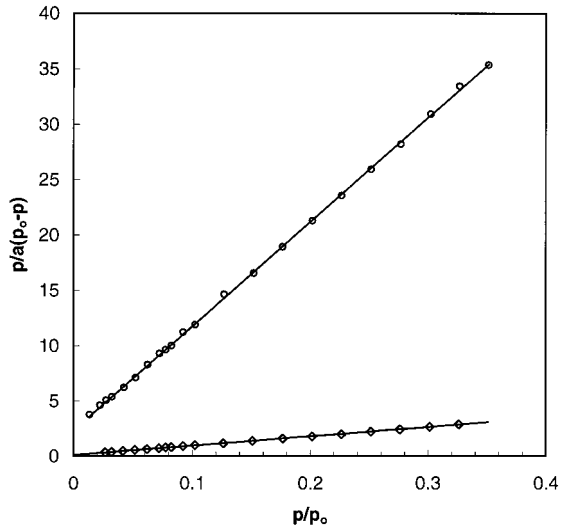

Figure 5. BET plot of nitrogen adsorption on bf at 77.4 K. Circles, C_{60}; diamonds, C_{60}/C_{70} bf. Line, linear regression.

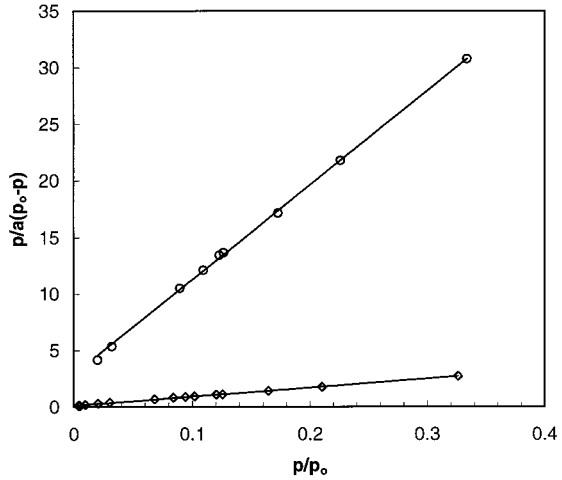

Figure 6. BET plot of argon adsorption on bf at 77.4 K. Circles, C_{60}; diamonds, C_{60}/C_{70} bf. Line, linear regression.

The combination of the values of the BET surface area and the helium pycnometry density allows to estimate the diameters of the equivalent spheres representing the average bf particle, $d \equiv 6/A^{BET}\cdot\rho_{bf}$. The above data yields $d_{C60} = 3.6$ μm and $d_{C60/C70} = 310$ nm and suggests that the C_{60} μm and C_{60}/C_{70} 200−800 nm particles observable in Figures 1 and 2 are most likely nonporous.

After the formation of the second adsorbed layer, the nitrogen adsorption isotherms exhibit a wide hysteresis loop, evidently due to the capillary condensation in the pores of the bf samples. Argon isotherms contain much less pronounced hystereses. It should be noted that transitions between molecular layers of argon are very smooth, unlike in the case of argon adsorption on gcb. In the latter case, the formation of each successive monolayer is signified by the steps on the adsorption isotherm.[13] This may suggest that the bf surface is more heterogeneous than that of gcb.

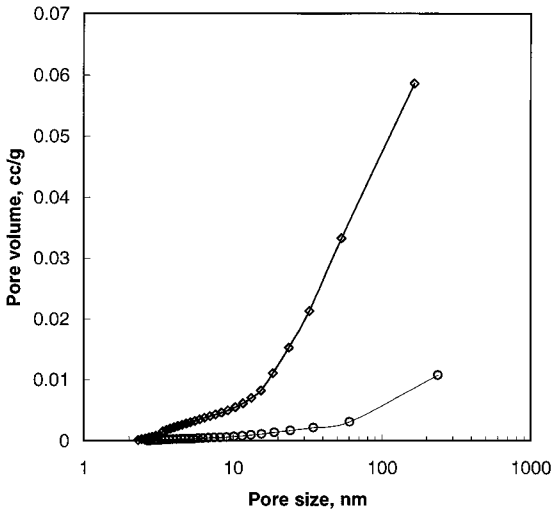

Figure 7. Pore size distribution of the C_{60} and C_{60}/C_{70} bf as determined by the BJH method from the nitrogen adsorption isotherms at 77.4 K.

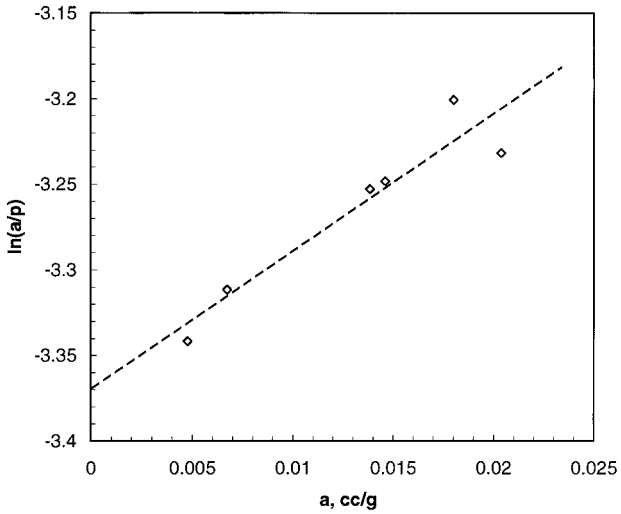

Figure 8. Virial plot of nitrogen adsorption on C_{60}/C_{70} bf at 77.4 K. Pressure P is used in Pa.

The porous structure of the bf samples was determined by applying the BJH method[32] to the multilayer part of the nitrogen adsorption isotherm (i.e., in the relative pressure range p/p_o of 0.35 to 1; see Figure 7). The pore size distribution is rather wide and spans the 3−200 nm range of the pore sizes, with the major part of the pore volume of C_{60} and C_{60}/C_{70} bf being accounted for by pores wider than 60 and 30 nm, respectively. It was observed earlier and shown below in the case of bf and gcb that the multilayer nitrogen adsorption is weakly dependent on the type of the substrate.[10] Therefore, the empirical t-curve derived from the so-called standard nitrogen adsorption isotherm and suitable for various substrates, including gcb,[10] was employed in the BJH method. The latter method employs model of cylindrical pores and neglects the pore connectivity, the effect of adsorption layer on the capillary condensate, and the capillary condensation hysteresis. In view of these assumptions and because of the decrease of the effect of adsorbed film on the pore size distribution in macropores, the use of the above t-curve is adequate for the purposes of this study. As was noted earlier,[10] the pore size distribution determined at relative pressure approaching unity should be treated carefully, since the small uncertainties in the temperature measurements could lead to a large error in the pore size determined by Kelvin-type approaches. In this study, the nitrogen adsorption measurements were quite reproducible at high p/p_o, and, therefore, the adsorbed amount and the pore volume were determined confidently throughout the whole pressure range. As suggested by the SEM images (Figures 1 and 2) and the bf specific volume-to-surface ratio, these pores are formed primarily by the spaces between the particles of the bf powder.

The second gas−solid surface virial coefficient B_{AS} was determined from the fit of the adsorption experimental data by the function of the virial equation of adsorption[8] in Henry's law limit:

$$\ln\left(\frac{a}{p}\right) = \ln\left(\frac{B_{AS}}{kT}\right) - 2\left(\frac{a}{A}\right)B_{2D} + K$$

Here k, T, A, and B_{2D} are the Boltzmann constant, absolute temperature, surface area, and second gas−solid surface virial coefficient. It was possible to obtain the low-pressure data that could reliably be fitted in Henry's law region only in the case of nitrogen adsorption on C_{60}/C_{70} bf sample. The intercept of the linear regression fit at zero a on the plot in Figure 8 yields the value of $B_{AS}^{C60/C70}$ to be in the range of 980 ± 80 cm^3/g (determined in four runs). In the case of nitrogen adsorption on gcb, this value was determined as $B_{AS}^{gcb} = 1824$ cm^3/g from the linear dependence of $\ln(B_{AS})$ on $1/T$.[33] To compare these two values, they should be reduced to a unit surface area of the solid. Such reduction, based on the value $A_{C60/C70}^{BET} = 11.7$ m^2/g and surface area determined independently for the gcb to be 19.7 m^2/g,[34] yields $B_{AS}^{C60/C70} = 84$ cm^3/m^2 and $B_{AS}^{gcb} = 93$ cm^3/m^2. Comparison of the latter two values suggests that in the low-pressure limit where the fluid−fluid interactions are negligible, the nitrogen interaction with the bf surface is similar to that with graphite. Alternatively, one may determine the bf surface area as the ratio of the second virial gas−solid coefficient determined for the unit mass of bf to that corresponding to the unit surface area of the gcb. The bf surface area evaluated in this way is $A_{C60/C70}^{BAS} = 10.7$ m^2/g.

The nitrogen and argon adsorption on C_{60} and C_{60}/C_{70} bf was compared to that on gcb using the comparative method.[10] In this method, the amounts of gas adsorbed on bf are plotted versus those on gcb surface at the same pressures and temperature (Figures 9 and 10). In this study, very reliable literature data[13,34] were used as the reference adsorption isotherms. It may be instructive first to examine nitrogen adsorption on bf in the range of 1 to 2−3 monolayers (as seen from Figure 3, at higher loadings nitrogen adsorption on the bf surface may be affected by capillary condensation). In the chosen range (see Figure 9) the nitrogen comparative plots on both bf become almost linear and, in agreement with the values of the second gas−solid virial coefficient, can be back-extrapolated into the origin of the coordinate system (Figure 9). This suggests that the multilayer adsorption of nitrogen on both bf is macroscopically similar to that on gcb. This notable feature is also suggestive of the absence of the micropores (i.e., pores of width less than 2 nm[10]) in the bf powder. The relative enhancement of the adsorption at the completion of the monolayer may be related to the two-dimensional fluid−solid transition of the adsorbed phase.[36]

As expected from the C_{60}/C_{70} second virial nitrogen−solid coefficient and as is the case of C_{60} bf, in the beginning of the submonolayer regime, the nitrogen comparative plots approach the origin of the coordinate system with a slope similar to that of the multilayer part of the comparative plot. This suggests that gas−solid interactions alone are quite similar on both studied bf. At slightly higher pressures and up to the completion of the first monolayer where fluid−fluid interactions may

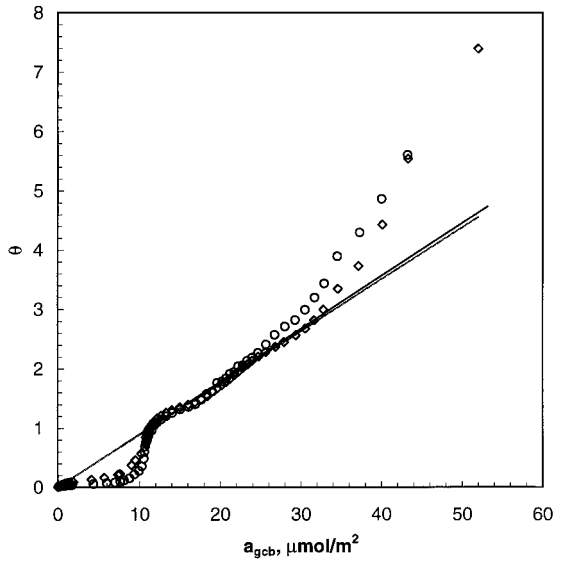

Figure 9. Nitrogen adsorption comparative plot at 77.4 K. Amount adsorbed on bf, θ in units of the monolayer capacity n_m, is plotted versus that on graphite a_{gcb}, mmol/m^2 [34] at the same pressures. Circles, C_{60}; diamonds, C_{60}/C_{70} bf. Line, linear regression.

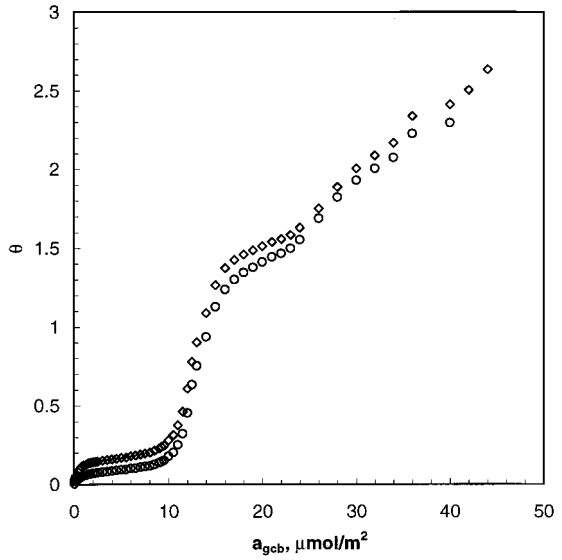

Figure 10. Argon adsorption comparative plot at 77.4 K. Amount adsorbed on the bf, θ in units of the monolayer capacity n_m, is plotted versus that on graphite a_{gcb}, mmol/m^2 [13] at the same pressures. Circles, C_{60}; diamonds, C_{60}/C_{70} bf. Line, linear regression.

enhance adsorption, the nitrogen amounts adsorbed on both bf are considerably smaller than on the gcb surface at the same pressure. This suggests that the strength of the interaction of nitrogen molecules with the bf surface is weaker than with the graphite surface in this adsorption range.

The argon comparative plots (Figure 10) are qualitatively quite similar to the nitrogen comparative plots. The argon adsorption is enhanced on bf relative to gcb at low pressures as opposed to the rest of the argon monolayer. The flattening of the plot is also observed at higher uptakes; however, its range is shifted into the higher pressure range and cannot be extrapolated back into the origin. This suggests that argon adsorption is weaker on bf than that on gcb in mono- and multilayer adsorption ranges.

The IR study of carbon monoxide and nitrogen oxide adsorption on bf crystals[24] suggests that there may be two active centers at the solid's surface: in the spaces between the fullerene molecules (strong) and on the top of the fullerene molecule (weak). Therefore, the observed form of the comparative plot in the monolayer range may be consistent with the adsorption on the strong adsorption centers of bf at low pressures, followed by the adsorption on the weak centers at higher pressures. As was mentioned in the Introduction, the gas atom−mirror image effect can be reduced in bf, and this may cause the lower overall adsorption activity of bf compared to gcb. However, as is suggested by the second gas−solid virial coefficient and the form of the initial part of the comparative plot, the gas adsorption on bf is as strong in Henry's law limit as on gcb. This may be the effect of the proximity of the carbon atoms in the interstices between the surface fullerene molecules and is reminiscent of the adsorption enhancement in the micropores of activated carbons.[10] However, in the case of nonporous bf crystals, this effect is limited to the surface of the bf crystal and is of lower magnitude.

While the physical properties of argon are similar to those of nitrogen, nitrogen atoms do have a considerable quadruple moment, while argon atoms do not. The observed nonspecific reduction of gas−solid interactions in the adsorption submonolayer thus corroborates nonspecificity of the gas−solid mirror image effect.[8] A better insight into the nature of the weakening of the adsorption in this regime can possibly be gained by studying adsorption on carbon nanotubes. The conductivity of the nanotubes can be reduced from metallic to semiconductor by changing the nanotube chirality (see, e.g., ref 35), with all other properties kept constant. Therewith, by comparing the submonolayer adsorption on nanotubes with different chirality, it may be possible to better quantify the mirror-image effect.

The bf surface area is proportional to the slope of the linear regression line of the multilayer part of the nitrogen comparative plot, and can be estimated from it as $A_{C60}^{comp} = 0.95$ m^2/g and $A_{C60/C70}^{comp} = 10.1$ m^2/g. The consistency of the bf surface areas determined by different methods (A^{BET}, A^{AS}, and A^{comp}) from nitrogen data supports the validity of the present analysis. It should be noted, however, that since the surface area of the gcb, used as a reference in calculations of A^{comp}, was itself determined by using the BET method, the values A^{BET} and A^{comp} are semi-independent.

One of the reviewers of this manuscript brought to our attention another study of nitrogen adsorption on bf.[25,26] In this earlier study, on the basis of the comparative method and the Dubinin−Radushkevich approach, it was concluded that bf may possess a small microporosity. However, it should be remembered that to use the comparative method for determination of the microporosity it was necessary to assume that the bf adsorption properties were identical to those of gcb. On the other hand, the use of the Dubinin−Radushkevich equation for the pore size determination is based on an empirical relationship, proposed for some activated carbons,[37] between the characteristic energy of adsorption and the pore size. Thus, an implicit assumption was made in the cited study that the bf properties were identical to those of some activated carbons. It was also noted earlier that the adsorption isotherms could be formally described by the Dubinin−Radushkevich equation even in the case of the nonporous adsorbents.[10] Therefore, the ability to fit the experimental adsorption isotherm using the Dubinin−Radushkevich equation alone should not be generally used as a criterion for establishing the existence of microporosity. Moreover, it is straightforward to show that fitting published nitrogen and argon adsorption isotherms measured on nonporous graphite with the Dubinin−Radushkevich function may supply the pore size distribution in the microporous range, similar to that found in refs 25 and 26. The present study is based on the measure-

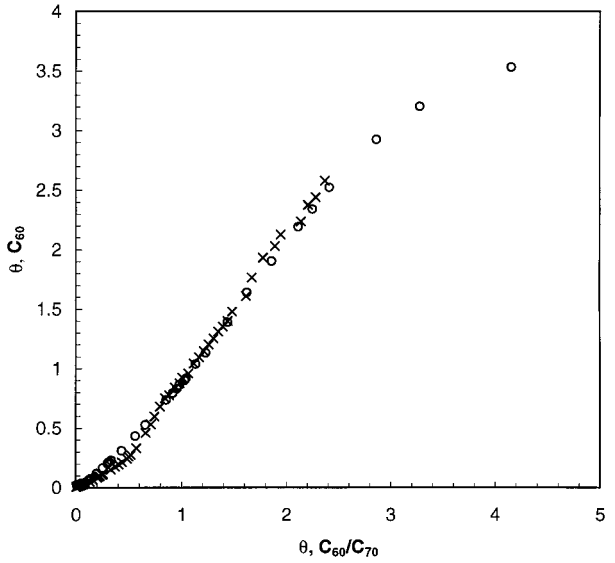

Figure 11. Nitrogen and argon adsorption comparative plots at 77.4 K. The amount adsorbed on C_{60} sample is plotted versus that on C_{60}/C_{70} bf, θ in units of the monolayer capacity n_m at the same pressures. Nitrogen, crosses; argon, circles.

ments that were done in two laboratories, with two types of bf samples, and two gases, and, in part, on independent data,[13,34] and does not allow to confirm the existence of the micropores in the fullerenes. Our findings, however, are in agreement with results of the work[22] in which no microporosity was found in bf. As is shown here, the properties of the bf surface are quite different from those of gcb surface, and, therefore, the gcb-based comparative method can be used only for quantitative analysis of the bf surface properties in the range above monolayer uptake.

Finally, we compare adsorption of nitrogen and argon on two studied bf samples. As suggested by the comparative plot shown in Figure 11, the two bf samples have quite similar adsorption properties throughout the whole adsorption uptake range. Considerable deviations appear only in the capillary condensation range becuase of the differences between the intersticial pore size distributions of the bf samples.

Conclusions

The C_{60} and C_{60}/C_{70} bf powders were found to consist of nonporous particles, characterized by 3 μm and 300 nm equivalent diameters and surface area of about 1.0 and 11 m^2/g, respectively. The nitrogen and argon affinity to the fullerenes is weaker than to the graphite in the major part of the monolayer, while in the low-pressure limit and in the multilayer regime the nitrogen adsorption on bf is macroscopically similar to that on graphite. This behavior is consistent with the possible bi-uniform character of the fullerene surface, and lessening of the gas−surface mirror image effect in fullerenes.

Acknowledgment. V.G. thanks E. Altman for productive correspondence. T. Bandosz and A. Bagreev are thanked for their help in argon measurements at City College of New York. The argon adsorption measurements were suggested by the reviewer. This work was supported in part by TRI/Princeton exploratory research grant.

References and Notes

(1) Dresselhaus, M. S.; Dresselhaus, G.; Eklund, P. C. *Science of Fullerenes and Carbon Nanotubes*; Academic Press: London, 1996.
(2) Kratschmer, W.; Lamb, L. D.; Fostropoulos, K.; Huffman, D. R. *Nature* **1990**, 347−354.
(3) Japan patent 06063396 A2.
(4) Li, D.; Swanson, B. I. *Langmuir* **1993**, *9*, 3341−3344.
(5) Synowczyk, A. W.; Heinze, J. In *Springer Series in Solid-State Sciences*; Kuzmany, H., Fink, J., Mehring M., Roth, S., Eds.; Berlin: Springer-Verlag: Berlin, 1993; Vol. 117, pp 73−7.
(6) Golovna, R. V.; Terenina M. B.; Ruchkina, E. L.; Karnatsevich, V. L. *Mendeleev Commun*. **1993**, 231−233.
(7) Eom, C. B.; Hebard, A. F.; Trimble, L. E.; Celler, G. K.; Haddon, R C. *Science* **1993**, *259*, 1887−1890.
(8) Steele W. A. *The Interactions of Gases with Solid Surfaces*; Pergamon: Oxford, 1974.
(9) Pierotti, R. A.; Thomas H. E. In *Surface and Colloid Science*; Matijevic, E. Ed.; Wiley-Interscience: New York, 1971; Vol. IV.
(10) Gregg, S. J.; Sing, K. S. W. *Adsorption, Surface Area and Porosity*; Academic Press: London, 1982.
(11) Gusev, V.; Seaton, N.; O'Brien, J. *Langmuir* **1997**, *13*, 2815−2821.
(12) Gusev, V.; O'Brien, J. *Langmuir* **1997**, *13*, 2822−2824.
(13) Avgul, N. N.; Kiselev, A. V. In *Chemistry and Physics of Carbon*; Marcel Dekker: New York, 1970; Vol. 6.
(14) Graham, D. *J. Phys. Chem*. **1957**, *61*, 1310.
(15) Putnam, F. A.; Fort, T. *J. Phys. Chem*. **1975**, *79*, 459.
(16) Everett, D. H. *Surface Area Determination*, Everett, D. H.; Otterwill, R. H., Eds.; Butterworth: London, 1970.
(17) Thomas, H. E.; Pierotti, R. A. *Trans. Faraday Soc*. **1973**, *7*, 1725.
(18) Dorset, D. L. *J. Phys. Chem*. **1996**, *100*, 16706−16710.
(19) Deitz, P.; Fostiropoulos, K.; Kratchmer, W.; Hansma, P. K. *Appl. Phys. Lett*. **1992**, *60*, 1 62.
(20) Chen, C. P.; Mehta, S.; Gasparini, F. M. *Physica B* **1994**, *194−196*, 879−880.
(21) Nemchuk, N. I.; Makarova, T. L.; Vul, A. Ya. *Fullerenes. Recent Advances in the Chemistry and Physics of Fullerenes and Related Materials*; Ruoff, R. S., Kadish, K. M., Eds.; Electrochemical Society: Pennington, NJ, 1996; Vol. III, PV 96−10, 464−473.
(22) Nagano, Y.; Kiyobayashi, T.; Nitta, T. *Chem. Phys. Lett*. **1994**, *217*, 186−190.
(23) Fastow, M.; Kozirovski, Y.; Folman, K.; Heidberg, J. *J. Phys. Chem*. **1992**, *96*, 6126−6128.
(24) Fastow, M.; Kozirovski, Y.; Folman, K. *Surf. Sci*. **1995**, *331−333*, 121−126.
(25) Kaneko, K.; Ishii, K.; Arai, T.; Suematsu, H. *J. Phys. Chem*. **1993**, *97*, 6764.
(26) Rostovtsev, R.; Ishii, C.; Wetoyama, N.; Uekawa, N.; Kaneko, K. *Adsorption* **1996**, *2*, 153−156.
(27) McLaughlan, A. D. *Mol. Phys*. **1964**, *7*, 381.
(28) Bruch L. W. *J. Chem. Phys*. **1983**, *79*, 3148.
(29) Ruoff, R. S.; Thornton, T.; Smith, D. *Chem. Phys. Lett*. **1991**, *186*, 456.
(30) Brunauer, S.; Emmet, P. H.; Teller, E. *J. Am. Chem. Soc*. **1938**, *60*, 39.
(31) Berezkina, Yu., F.; Dubinin, M. M.; Sarahov, A. I. *Bull. USSR Academy of Sciences, Section Chemistry* **1969**, 2495.
(32) Barrett, E. P.; Joyner, L. G.; Halenda, P. H. *J. Am. Chem. Soc*. **1951**, *73*, 373.
(33) Bojan, M. J.; Steele W. A. *Langmuir* **1987**, *3*, 1123−1127.
(34) Isirikian, A. A.; Kiselev, A. V. *J. Phys. Chem*. **1961**, *65*, 601−607.
(35) Eletskii, A. V. *Phys.-Uspekhi* **1997**, *80*, 899−924.
(36) Piper, J.; Morrison, J. A.; Peters, C.; Ozaki, Y. *J. Chem Soc., Faraday Trans. 1* **1983**, *79*, 2863−2874.
(37) Dubinin, M. M. *Adsorption in Micropores*; Nauka: Moscow, 1983; 183 p.